Quasi-shear waves in inhomogeneous weakly anisotropic media by the quasi-isotropic approach: a model study [1] [2]

Ivan Pšenčík* and **Joe Dellinger****

* *Geophysical Institute, Acad. Sci. of Czech Republic, Boční II, Praha 4, Czech Republic*
e-mail: ip@ig.cas.cz

** *BP Amoco, 501 Westlake Park Blvd, Houston, TX 77079, U.S.A.*
e-mail: dellinja@bp.com

(April, 2000)

ABSTRACT

In inhomogeneous isotropic regions, *S* waves can be modeled using the ray method for isotropic media. In inhomogeneous *strongly anisotropic* regions, the independently propagating *qS1* and *qS2* waves can similarly be modeled using the ray method for anisotropic media. The latter method does not work properly in inhomogeneous *weakly anisotropic* regions, however, where the split *qS* waves couple. The zeroth-order approximation of the quasi-isotropic (QI) approach was designed for just such inhomogeneous weakly anisotropic media, for which neither the ray method for isotropic nor anisotropic media applies.

We test the ranges of validity of these three methods using two simple synthetic models. Our results show that the QI approach more than spans the gap between the ray methods: it can be used in isotropic regions (where it reduces to the ray method for isotropic media), in regions of weak anisotropy (where the ray method for anisotropic media does not work properly), and even in regions of moderately strong anisotropy (in which the *qS* waves decouple and thus could be modeled using the ray method for anisotropic media). A modeling program that switches between these three methods as necessary should be valid for arbitrary-strength anisotropy.

INTRODUCTION

It is well known that the ray method for inhomogeneous anisotropic media yields distorted results (or fails to produce any result at all) for *qS* waves propagating in inhomogeneous *weakly anisotropic* media. It also does not work properly in the vicinity of *qS*-wave singularities, which all *qS* modes possess. In both these cases the problem is caused by coupling

[1]Presented at the 68th Annual Meeting of the Society of Exploration Geophysicists

[2]Seismic Waves in Complex 3-D Structures, Report 10 (Department of Geophysics, Charles University, Prague 2000), pp.203-225

between the qS-waves at inhomogeneities in the medium. The coupling violates the ray method's implicit assumption that each studied wave is isolated and independent. While inhomogeneity always causes some coupling, if the elastic parameters are slowly varying along the ray and the qS-wave phase velocities are not close, the coupling is negligible and can be ignored, and the ray method can safely be applied. However, if the elastic parameters vary quickly and the phase velocities are similar, the coupling is significant, the waves cannot be treated independently, and application of the ray method leads to incorrect results (as we demonstrate in this paper).

To avoid these problems, the so-called *quasi-isotropic (QI) approach* was proposed by Kravtsov (1968). [See also Kravtsov & Orlov (1980), Pšenčík (1998a,b), and Červený (2000).] In the QI approach, the asymptotic solution of the elastodynamic equation is sought in the form of an expansion with respect to two small parameters of the same order. The first is the same small parameter used in the standard ray method, $\epsilon_1 \sim c/\omega L$, where ω is the circular frequency, c is the phase velocity, and L is the characteristic length (i.e., the shortest distance on which the quantities related to wave propagation change by an amount comparable to their own magnitude). The second parameter, $\epsilon_2 \sim ||\Delta a_{ijkl}||/||a_{ijkl}|| \sim \Delta c/c$, characterizes the strength of the anisotropy. Here a_{ijkl} is the tensor of density-normalized elastic stiffnesses, and Δa_{ijkl} is the difference between a_{ijkl} and the corresponding tensor of density-normalized elastic stiffnesses of an *isotropic* reference medium.

Physically, ϵ_2 is a measure of the difference between the phase velocities of the split qS waves propagating along the ray. If $\epsilon_2 = 0$, the medium is isotropic and the ray method for isotropic media applies. If ϵ_2 is large, such that $\epsilon_2 \gg \epsilon_1$, the split qS waves are well separated and can be dealt with independently using the ray method for anisotropic media. The QI approach was designed to handle the intermediate case, $0 \leq \epsilon_2 \leq \epsilon_1$. [Note the zeroth-order approximation of the QI approach is equivalent to the coupling ray theory (CRT) of Coates & Chapman (1990); see Pšenčík (1998a) for a proof.]

Our goal in this paper is to test how well the QI approach actually performs in weakly anisotropic media. In the process we will attempt to illuminate two important practical questions left unanswered by previous (more theoretically oriented) studies: 1) What happens if we apply the QI approach to moderately anisotropic media (for which $\epsilon_2 \geq \epsilon_1$, but not $\epsilon_2 \gg \epsilon_1$)? 2) How badly does the ray method for anisotropic media break down if we attempt to apply it to qS waves in weakly anisotropic media (for which $\epsilon_2 < \epsilon_1$)?

To study these questions, we used an updated version of the program ANRAY (Gajewski & Pšenčík, 1990) to model qS-wave propagation in two synthetic offset VSPs. In both models we considered vertically *inhomogeneous* weakly anisotropic HTI (Transversely Isotropic with a Horizontal axis of symmetry) media, with the symmetry axis of the HTI anisotropy rotated 45° from the plane defined by the source-receiver offsets of the VSP. The two models differed only in the strength of the anisotropy. In the first ("VWA") the anisotropy was so weak (0.02-0.1%) that the medium was effectively isotropic. In the second ("WA") the anisotropy was considerably stronger, but still "weak" (1-4%). For each model we performed the calculation using three different asymptotic methods: the zeroth-order approximation of the ray method for isotropic media (ISO), the zeroth-order approximation of the ray method for anisotropic media (ANI), and the zeroth-order approximation of the QI approach (henceforth simply called “QI”). As a “reality check”, we also calculated the seismograms using a non-ray algorithm, the anisotropic reflectivity modeling program Anivec^{TM} (Mallick & Frazer, 1990).

Examination of the results for the VWA model shows that the ray method for anisotropic media (ANI) does not properly describe qS-wave propagation in weakly anisotropic media, a result consistent with theory. Comparing the QI, ISO, and ANI results for the WA model, we find that the QI results can resemble either the ISO or ANI results, depending on the local strength of the anisotropy and the dominant frequency of the wavelet (and thus on the relative magnitudes of ϵ_1 and ϵ_2). The comparison confirms theoretical expectations that the QI approach should represent a link between the ray methods for isotropic and anisotropic media. Although ANRAY and Anivec differ in their model-specification options, so their respective computations could not be made precisely equivalent, we also found there was a good fit between the full-wave-equation seismograms generated by Anivec and the weak-anisotropy QI ray-tracing results generated by ANRAY.

METHODOLOGY OF THE QI APPROACH

To implement the QI method, we begin by defining a reference isotropic medium, obtaining the necessary P and S-wave velocities by averaging the qP, $qS1$ and $qS2$ phase velocities of the true weakly anisotropic medium over a range of propagation directions (Rasolofosaon et al., 1991). A ray connecting the source and receiver is then calculated in the reference isotropic medium, and dynamic ray tracing is performed along this ray to determine the geometrical spreading of the S wave in the isotropic medium. The novel part of the algorithm is the determination of the QI amplitudes. These are obtained by solving two coupled linear ordinary differential equations along the ray in the isotropic reference medium (equation (A-7) in appendix A) for selected frequencies within the desired wavelet frequency band. Using the resulting *frequency-dependent* QI amplitudes, a frequency response is calculated, which is then used to construct the required wavelet for the output vector seismogram. See Appendix A for more specific mathematical details about the QI algorithm.

NUMERICAL TESTS

For the following tests we use the VSP configuration shown schematically in Figure 1. The source, a vertical point force directed downwards, is situated at the point S on the surface, 1 km from the mouth of the borehole. The effects of the free surface are neglected throughout. The source time function, a windowed symmetric Gabor wavelet, is shown in Figure 2. There are 29 receivers in the borehole, distributed with a uniform step size of 0.02 km, with receiver depths ranging from 0.01 km to 0.57 km. The 3-component receivers record the vertical (positive downwards), transverse, and radial (positive away from the source) components of the wave field. The recording system is right-handed. All calculated seismograms and particle-motion diagrams are shown with no differential scaling between components and traces, so true relative amplitudes can be seen.

In both models, the medium is vertically inhomogeneous and transversely isotropic with a horizontal axis of symmetry (HTI). In the first, taken from a study of Coates & Chapman (1990), the anisotropy is very weak; for the frequencies used, the model is essentially isotropic. We call this model "VWA" (Very Weak Anisotropy). The anisotropy in the second model, "WA" (Weak Anisotropy), is stronger so that some effects of shear-wave splitting can be observed. In both models, the symmetry axis of the azimuthally anisotropic HTI medium is rotated 45° out of the vertical plane containing the source and the borehole. (We will call this the "propagation plane", even though the rays may not propagate exactly within this plane because of the azimuthal anisotropy.) The HTI symmetry axis is given by the vector $(\frac{1}{2}\sqrt(2), \frac{1}{2}\sqrt(2), 0)$.

The VWA model

In the coordinate system with the axis of symmetry parallel to the $x-$axis, the matrices of density-normalized elastic parameters A_{ij}, in units of (km/s)^2, for the VWA model are as follows: At a depth of 0. km,

$$\begin{pmatrix} 20.248 & 7.457 & 7.457 & 0.000 & 0.000 & 0.000 \\ & 20.250 & 7.448 & 0.000 & 0.000 & 0.000 \\ & & 20.250 & 0.000 & 0.000 & 0.000 \\ & & & 6.401 & 0.000 & 0.000 \\ & & & & 6.386 & 0.000 \\ & & & & & 6.386 \end{pmatrix}$$

and at a depth of 1. km,

$$\begin{pmatrix} 30.878 & 11.372 & 11.372 & 0.000 & 0.000 & 0.000 \\ & 30.881 & 11.358 & 0.000 & 0.000 & 0.000 \\ & & 30.881 & 0.000 & 0.000 & 0.000 \\ & & & 9.762 & 0.000 & 0.000 \\ & & & & 9.739 & 0.000 \\ & & & & & 9.739 \end{pmatrix}.$$

(A rotation of 45° about the $z-$axis has to be carried out to obtain the actual model.) The elastic parameters between the depths of 0. and 1. km are determined by linear interpolation. Since in this medium the anisotropy is factorizable (i.e., $\mathbf{A}(z) = (f(z)/f(0))\,\mathbf{A}(0)$), the Thomsen parameters (here referenced to the x axis instead of the usual z) are constant throughout: $\epsilon = (A_{33} - A_{11})/(2A_{11}) = .0000494$, $\gamma = (A_{44} - A_{66})/(2A_{66}) = .00117$, and $\delta = ((A_{13} + A_{66})^2 - (A_{11} - A_{66})^2)/(2A_{11}(A_{11} - A_{66})) = -.000938$. The density, 1.0 g/cm^3, is also constant throughout. Sections of the qS-wave phase-velocity surfaces in the vertical propagation plane for depths of 0.0 and 0.6 km are shown in Figure 3. Note that although the model is nearly isotropic, it does contain an intersection singularity. The qS anisotropy shown in the figure (defined as $(c_{qS1} - c_{qS2})/c_{\text{average}}$, where c denotes phase velocity) varies from 0.02% for horizontal propagation to 0.1% for vertical propagation.

The upper part of Figure 4 shows ray diagrams, time-distance, and amplitude-distance curves for the two qS waves in the VWA medium, calculated using the ray method for anisotropic media (ANI). The bottom part of Figure 4 shows the same quantities for the S wave in the isotropic reference medium, calculated using the ray method for isotropic media (ISO). The left column in each subfigure shows, from bottom to top, two ray diagrams (projected onto the vertical propagation plane, and onto the horizontal plane), and a graph of traveltimes versus receiver depth. The right column shows base-10 logarithms of the recorded ray amplitudes, generated by the vertical point-force source, as a function of receiver depth (from bottom to top, for the vertical, transverse, and radial components).

We can see that in the isotropic medium, rays to all receivers were found and these rays were confined to the plane of propagation. Note especially that the generated S wave has a pure SV polarization, so the amplitude of its transverse component (shown in the "empty box" in Figure 4) is identically zero. In contrast, in the anisotropic medium the rays did not illuminate all the receivers. The reason is a breakdown of the ray tracer due to the shear-wave singularity shown in Figure 3, which was encountered by the rays arriving at the deepest receivers. At a singularity, the denominators of the right-hand sides of the ray-tracing equations become zero (see Gajewski & Pšenčík, 1990), causing the calculation to abort. The ray diagrams and traveltime curves for both qS waves are nearly identical to the corresponding parts of the ray diagram and traveltime curve for the S wave in the isotropic reference medium; this is due to the closeness of the anisotropic VWA medium to the isotropic one. There is, however, a remarkable difference in the behavior of the ray amplitudes: neither of the two qS waves in the ANI section is purely SV or SH polarized. In a medium that is so nearly isotropic, a vertical force should have only been able to generate a nearly purely SV-polarized shear wave. The ray method for anisotropic media thus gave an *incorrect* result in this example.

Figure 5 shows synthetic seismograms for the VWA model of Figure 3 calculated in three different ways. From left to right, they are for S waves calculated using the ray method for isotropic media (ISO), qS waves calculated using the QI approach, and qS waves calculated using the ray method for anisotropic media (ANI). The dominant frequency of the source-time function is 50 Hz. Examining the ANI results, we again see that the ray method for anisotropic media incorrectly yielded a wave with a rather strong transverse component (arrowed); the transverse component is, in fact, stronger than the radial one. Seismograms for the deeper receivers in the ANI section are missing because of the breakdown of the ray-tracing procedure. As expected, the ISO results show an identically zero transverse component. The QI results very closely resemble the ISO results; although some disturbances are visible on the transverse component, they have negligible amplitudes.

Figure 6 shows hodograms calculated using the three methods for the receivers at depths of $z = 0.01$ km ("shallow"), 0.29 km ("intermediate"), and 0.57 km ("deep"). Since the particle motion at the receiver is three dimensional, three two-dimensional projections are shown for each result. In the ISO result (left), the polarization of the S-wave arrival is strictly linear. The bottom row of plots shows the polarization of the arriving wave in the vertical propagation plane; note that for the shallow receiver the S wave arrives from below, a result of the vertical velocity gradient. The top row of plots shows the polarization in the horizontal plane; it is purely SV polarized for all three receivers.

The center set of hodograms in Figure 6 shows the results of the QI approach. Only small deviations from the corresponding ISO results are evident; most noticeably, the particle motion displays a small amount of quasi-ellipticity. The polarization is, however, still overwhelmingly SV. In contrast, the right (ANI) set of hodograms in Figure 6 differs from the others in two significant ways. First, due to the previously mentioned breakdown of the ray tracer, there are no observations for the deepest receiver. Second, although the arrivals are linearly polarized, the hodograms show a significant SH component of displacement, indicating that even before the ray method failed it was not producing correct results. We conclude that since the QI method did correctly reproduce the ISO results, it performed well in this very weakly anisotropic model, despite having to propagate rays through a region containing an intersection singularity.

The WA model

In the coordinate system with the axis of symmetry parallel to the $x-$axis, the matrices of density-normalized elastic parameters A_{ij}, in units of (km/s)^2, for the WA model are as follows: At a depth of 0. km,

$$\begin{pmatrix} 13.39 & 4.46 & 4.46 & 0.00 & 0.00 & 0.00 \\ & 15.71 & 5.04 & 0.00 & 0.00 & 0.00 \\ & & 15.71 & 0.00 & 0.00 & 0.00 \\ & & & 5.33 & 0.00 & 0.00 \\ & & & & 4.98 & 0.00 \\ & & & & & 4.98 \end{pmatrix}$$

and at a depth of 1. km,

$$\begin{pmatrix} 20.42 & 6.80 & 6.80 & 0.00 & 0.00 & 0.00 \\ & 23.96 & 7.69 & 0.00 & 0.00 & 0.00 \\ & & 23.96 & 0.00 & 0.00 & 0.00 \\ & & & 8.13 & 0.00 & 0.00 \\ & & & & 7.60 & 0.00 \\ & & & & & 7.60 \end{pmatrix}.$$

As before, the elastic parameters between the depths of 0. and 1. km are determined by linear interpolation. The density is a uniform 1.0 g/cm^3. The Thomsen parameters (referenced to the x axis) are constant throughout: $\epsilon = (A_{33} - A_{11})/(2A_{11}) = .0866$, $\gamma = (A_{44} - A_{66})/(2A_{66}) = .0351$, and $\delta = ((A_{13} + A_{66})^2 - (A_{11} - A_{66})^2)/(2A_{11}(A_{11} - A_{66})) = .0816$. The orientation of the symmetry axis is exactly as in the previous (VWA) model. Figure 7 shows vertical sections through the qS-wave phase-velocity surfaces in the propagation plane for model depths of 0.0 and 0.6 km. Note the anisotropy is stronger than in the previous example, varying from 1% for horizontal propagation up to 4% for vertical propagation.

Figure 8 shows synthetic seismograms for the WA model, again calculated using a source with a dominant frequency of 50 Hz; the only change from Figure 5 is the stronger anisotropy. This time the QI results more closely resemble the results of the ray method for anisotropic media (ANI), especially for the deeper receivers, not the ray method for isotropic media (ISO) as was the case for the VWA model in Figure 5. This is because of the stronger anisotropy in the WA model, combined with the relatively high dominant frequency of the source wavelet. In particular, note that in the ANI and QI results in Figure 8, two shear-wave arrivals can be observed: first a fast shear wave with predominantly SV polarization, followed by a slower one with predominantly SH polarization. The QI approach can thus model shear-wave splitting, even though it is based on calculations taking place along a single ray calculated in the *isotropic* reference medium.

Figure 9 shows hodograms constructed for the same three receivers as those used for the VWA experiment in Figure 6. In Figure 9, the particle motions calculated using the QI approach (center) do not uniformly match the ISO set of hodograms (left). Instead, the particle motions calculated by the QI method are nonlinear for the intermediate and deep receivers, indicating the presence of interfering waves. For the deeper receivers, the particle motions calculated using the QI method closely resemble those calculated using the ANI method (right). For the shallow receiver, however, the QI method does still produce a particle motion differing only slightly from its "isotropic" counterpart.

In Figure 9 the QI approach thus converged to the "isotropic" result for the shallow receiver, while for the deeper receivers it converged to the "anisotropic" result. This happened because for the shallow receiver the difference between the two qS-wave phase velocities was smaller than it was for the deeper receivers (see Figure 7), and also because the waves traveled a shorter distance from the source to get to the shallow receiver, and so had less time to "split". The qS waves thus propagated to the shallow receiver through a medium that more closely resembled an isotropic one. On the other hand, the pronounced quasi-elliptical polarization recorded by the deeper receivers is a consequence of shear-wave splitting, indicating propagation through a more effectively anisotropic medium.

While the quasi-elliptical polarization in the ANI results in Figure 9 is a natural consequence of interference between two qS waves independently propagating along two different ray paths, its origin in the QI results is not so straightforward. The quasi-elliptical polarization in the QI results is a consequence of solving the two coupled differential equations (A-7) along the single ray calculated for an S wave in the reference isotropic medium. Once the split shear waves have finished separating, as they have almost done by the time they reached the deepest receiver in Figure 9, the QI approach could, in principle, be dropped in favor of the standard ray method for anisotropic media. From that point on, two qS waves could be calculated along two different ray paths, even in this weakly anisotropic medium.

Figure 10 shows the effects of reducing the dominant frequency of the source wavelet to 10 Hz (the ISO results would look exactly the same as in Figure 9, and so are not plotted). The hodograms for the QI approach now look more like the results of the ray method for isotropic media in Figure 9: the particle motions at the intermediate and deep receivers are still slightly nonlinear, but now are (for the most part) confined to the plane of propagation (see the transverse-vertical and transverse-radial diagrams). Reducing the dominant source frequency even further would eventually lead to linear polarizations indistinguishable from those in the ISO results in Figure 9. Reducing the source frequency would also lead to linear polarizations in the ANI results on the left, but a non-negligible transverse component would remain, which is incorrect.

Increasing the source frequency to 200 Hz leads to a closer resemblance between the QI and the ANI results, as can be seen in Figure 11. (In this figure we finally have $\epsilon_2 \geq \epsilon_1$ for most of the frequencies present; for these frequencies the assumptions underlying the ray method for anisotropic media should be valid.) The qS waves at the intermediate and deep receivers are now clearly separated, and the independent qS waves display linear polarizations in both the QI and ANI results. The ISO results for this frequency would still look exactly the same as in Figure 9.

Comparison with a non-asymptotic result

In Figure 12, the seismograms calculated for the VWA and WA models using the QI approach are compared with the seismograms calculated by Anivec$^{\mathrm{TM}}$, a commercial implementation of the reflectivity method for anisotropic media (Mallick & Frazer, 1990). The left column shows synthetic seismograms for the VWA model, the right column seismograms for the WA model. The QI synthetics are shown by the black lines, the reflectivity synthetics by the gray lines. Since the algorithms and implementations used were entirely distinct, there were some unavoidable differences in the specifications of the model and the source between the reflectivity and QI calculations. For the reflectivity model, the continuous vertical gradient used in the QI computations had to be simulated using homogeneous layers. We used one hundred layers, each 10 m-thick (about 10 times finer than the dominant wavelength of the seismic energy of interest). A spike multiplied by a cosine taper spanning 5 Hz to 100 Hz in the frequency domain was used for the wavelet, to approximately match the wavelet for the QI computation shown in Figure 2.

Despite these differences, the reflectivity and QI seismograms are very similar; the synthetics nearly coincide for most receivers. It's not clear whether the differences that are visible are due to the limitations of the QI approach or the reflectivity method, or both. (The slight phase shift on the vertical and transverse components will be a subject of further study.) It should also be noted that because the model was azimuthally anisotropic, the reflectivity method required an expensive two-dimensional integration in the slowness domain; the reflectivity results in Figure 12 represent several thousand times the computational effort of the corresponding QI synthetics! The QI approach is also applicable to laterally inhomogeneous media, while reflectivity methods are limited to vertically inhomogeneous media only.

DISCUS]SION

We have demonstrated that the zeroth-order approximation of the ray method for anisotropic media cannot properly describe the coupling of qS waves in media which are effectively isotropic. The QI approach, however, performs well in such media. This suggests that the QI approach might be applicable not just to waves propagating in weakly anisotropic media (such as the VWA and WA models examined in this paper), but also to waves passing near shear-wave singularities in more strongly anisotropic media. The VWA model results presented here did demonstrate that the QI approach can work for a ray passing through an intersection singularity in a weakly anisotropic medium, a situation that caused the ray method for anisotropic media to break down.

Possible applications of the QI approach to singular regions in strongly anisotropic media is a task for another study. In strongly anisotropic media the QI approach would not be used continuously, but only as a fallback for when the ray method was in danger of producing an incorrect or inaccurate result. The isotropic reference medium could then be chosen dynamically, so as to match the local qP and qS velocities associated with the slowness direction of the current ray. The optimal choice of isotropic reference media in the QI approach is also a subject for future study.

All the computations presented in this paper were performed using the zeroth-order approximation of the QI approach. Since the anisotropy of the considered models was rather weak, the absence of the first-order additional terms did not significantly affect the results of the QI approach. The effects of the first-order terms would be most visible in the vertical-radial plane of the particle-motion diagrams. In Figure 9, the more strongly anisotropic model of the two considered, the projections of the particle motion onto this plane have almost identical orientations for all three methods, indicating that the zeroth-order approximation was sufficient for these models.

The simple models considered in this study were sufficient to demonstrate the basic effects of frequency and strength of anisotropy on the coupling of qS waves; the qS waves decouple both with increasing frequency and with increasing strength of anisotropy or, equivalently, with increasing distance over which the split qS waves have propagated and increasing difference between the split qS waves' phase velocities. Some inhomogeneity is necessary for qS waves to become coupled; in a completely homogeneous medium, elastic waves can be decomposed into a sum of pure-mode waves, all of which propagate independently. In this paper, we restricted ourselves to a simple form of inhomogeneity, a linear variation of the elastic parameters with depth. Studies of how varying the strength of the inhomogeneity affects the coupling of qS waves will be one of the next steps in the analysis of the QI approach.

CONCLUSIONS

We have presented numerical results obtained using the zeroth-order approximation of the QI approach for qS waves in inhomogeneous weakly anisotropic media. The results confirm that the QI approach does represent a link between the ray methods for isotropic and anisotropic media, as was expected from theoretical studies. In a model with very weak anisotropy, the QI approach gave results which effectively coincided with the results of the ray method for isotropic media. When stronger anisotropy and higher frequencies were considered, the results of the QI approach converged to the results of the ray method for *anisotropic* media. The region of applicability of the QI approach thus appears to overlap the regions of applicability of both the ray method for isotropic media and the ray method for anisotropic media as well. Within its own region of applicability, the zeroth-order approximation of the QI approach models the behavior of strongly coupled qS waves, something that cannot be done using the zeroth-order approximations of either of the ray methods. A modeling program that switches between the three methods as necessary should be valid for arbitrary strengths of anisotropy. We plan to perform further comparisons with wave-equation methods to test the accuracy of the QI approach.

ACKNOWLEDGMENTS

The authors are indebted to Prof. V. Červený and L. Klimeš for many useful discussions. Critical reviews of V. Vavryčuk, L. J. Martins and two anonymous reviewers are also appreciated. This work was supported by the consortium project "Seismic waves in complex 3-D structures (SW3D)", by the EC, INCO - Copernicus Project IC15 CT96 200, and by the Grant Agency of the Czech Republic, Grant No. 205/96/0968.

REFERENCES

Červený, V., 2000, Seismic ray theory: Cambridge University Press, Cambridge.

Coates, R. T. & Chapman, C. H., 1990, Quasi-shear wave coupling in weakly anisotropic 3-D media: Geophys. J. Int., **103**, 301-320.

Gajewski, D. & Pšenčík, I., 1990, Vertical seismic profile synthetics by dynamic ray tracing in laterally varying layered anisotropic structures: J. Geophys. Res., **95**, 11301-11315.

Kravtsov, Yu. A., 1968, "Quasi-isotropic" approximation to geometrical optics: Dokl. AN SSSR, **183**, No.1, 74-77 (in Russian).

Kravtsov, Yu. A. & Orlov, Yu. I., 1980, Geometrical optics of inhomogeneous media: Nauka, Moscow (in Russian).

Mallick, S. & Frazer, L. N., 1990, Computation of synthetic seismograms for stratified azimuthally anisotropic media, J. Geophys. Res., **86**, 359-377.

Popov, M. M. & Pšenčík, I., 1978, Computation of ray amplitudes in laterally inhomogeneous media with curved interfaces: Studia geoph. et geod., **22**, 248-258.

Pšenčík, I., 1998a, Green's functions for inhomogeneous weakly anisotropic media: Geophys. J. Int., **135**, 279-288.

Pšenčík, I., 1998b, Quasi-isotropic approximation of the qS wave Green function: 68th Ann. Internat. Mtg., Soc. Expl. Geophys., Expanded Abstracts, 1795-1798.

Rasolofosaon, P., Arts, R. J., and Helbig, K., 1991, General anisotropic elastic tensor in rocks: approximation, invariants, and particular directions: 61st Ann. Internat. Mtg., Soc. Expl. Geophys., Expanded Abstracts, 1534-1537.

APPENDIX A - BASIC QI FORMULAE

We briefly review here the basic formulae used when calculating the zeroth-order approximation of the QI approach. For more details see Pšenčík (1998a,b). We will follow the standard conventions of the ray-tracing literature: If a subscript is repeated, there is an implied summation over it (e.g. $x_i y_i \rightarrow \sum_i x_i y_i$). δ_{ij} is the Kronecker delta; it is zero unless its two subscripts have the same value, in which case it is one (e.g. $\delta_{12} = 0$, $\delta_{22} = 1$). Vectors and tensors are referred to by their individual scalar components (e.g. $a_{ijkl} \rightarrow \mathbf{A}$). Subscripts are reserved for components (e.g. $x_i \rightarrow \{x_1,\, x_2,\, x_3\} \rightarrow \mathbf{x}$), while superscripts in parenthesis are used to distinguish between corresponding quantities (e.g. $qS^{(I)} \rightarrow \{qS^{(1)},\, qS^{(2)}\}$). A comma before a component indicates partial differentiation (e.g. $u_{i,j} \rightarrow \partial u_i / \partial x_j$).

Begin by considering the tensor of density-normalized stiffness parameters for a weakly anisotropic media a_{ijkl}, such that

$$a_{ijkl} = a^0_{ijkl} + \Delta a_{ijkl} \quad . \tag{A-1}$$

The tensor a^0_{ijkl} gives the stiffness parameters of a reference isotropic medium:

$$a^0_{ijkl} = (\alpha^2 - \beta^2)\delta_{ij}\delta_{kl} + \beta^2(\delta_{ik}\delta_{jl} + \delta_{il}\delta_{jk}) \quad , \tag{A-2}$$

where α and β denote its P- and S-wave velocities, respectively. The Δa_{ijkl} then specify how the weakly anisotropic medium deviates from the reference isotropic medium, which should be chosen so that $|\Delta a_{ijkl}|$ is as small as possible.

In the zeroth-order approximation of the QI approach, the qS-wave Green's function is given by

$$G_{in}(\tau, \tau_0, \omega) = \exp(i\omega\tau)\Big[\mathcal{B}_n(\tau, \omega)e_i^{(1)}(\tau) + \mathcal{C}_n(\tau, \omega)e_i^{(2)}(\tau)\Big] \ , \tag{A-3}$$

simultaneously incorporating both shear waves; see Pšenčík (1998a). The subscript n specifies that the vector Green's function G_i is for a unit-vector point-force source oriented along the x_n axis. The symbol τ_0 denotes the time at the source; $\tau - \tau_0$ is the traveltime along the ray of the S wave in the reference isotropic medium. The vectors $e_i^{(k)}$ define an orthogonal ray-centered coordinate system. $e_i^{(3)}$ is a unit vector tangent to the ray; mathematically,

$$e_i^{(3)} = \beta\, \tau_{,i} \ . \tag{A-4}$$

The unit vectors $e_i^{(1)}$ and $e_i^{(2)}$ represent the polarization vectors of an S wave in the reference isotropic medium, and are perpendicular both to the ray and each other. They satisfy the equation

$$\frac{de_i^{(I)}}{d\tau} = (\beta_{,k}\, e_k^{(I)})\, e_i^{(3)} \ ; \tag{A-5}$$

see e.g. Popov & Pšenčík (1978), Červený (2000).

The terms $\mathcal{B}_n(\tau,\omega)$ and $\mathcal{C}_n(\tau,\omega)$ are the amplitudes of the qS waves in the zeroth-order approximation of the QI approach. They have the form

$$\mathcal{B}_n(\tau,\omega) = \frac{\bar{\mathcal{B}}_n(\tau,\omega)}{\sqrt{\rho(\tau)\beta(\tau)\Omega_M(\tau)}}, \qquad \mathcal{C}_n(\tau,\omega) = \frac{\bar{\mathcal{C}}_n(\tau,\omega)}{\sqrt{\rho(\tau)\beta(\tau)\Omega_M(\tau)}} \ . \tag{A-6}$$

The symbol ρ denotes the density. The quantity Ω_M is obtained from the dynamic ray tracing in the background isotropic medium; its magnitude $|\Omega_M|$ gives the relative geometrical spreading. Equations (A-6) would represent zeroth-order ray solutions for qS waves if the terms $\bar{\mathcal{B}}_n$ and $\bar{\mathcal{C}}_n$ were constant. In the zeroth-order approximation of the QI approach, however, the terms $\bar{\mathcal{B}}_n$ and $\bar{\mathcal{C}}_n$ depend on τ and frequency ω, and are obtained as solutions of two coupled linear ordinary differential equations of the first order:

$$\frac{d\bar{\mathcal{B}}_n}{d\tau} = -\frac{1}{2} i\omega\beta^{-2}(B_{11}\bar{\mathcal{B}}_n + B_{12}\bar{\mathcal{C}}_n), \qquad \frac{d\bar{\mathcal{C}}_n}{d\tau} = -\frac{1}{2} i\omega\beta^{-2}(B_{12}\bar{\mathcal{B}}_n + B_{22}\bar{\mathcal{C}}_n) \ , \tag{A-7}$$

with initial conditions

$$\bar{\mathcal{B}}_n(\tau_0) = \frac{e_n^{(1)}(\tau_0)}{4\pi\sqrt{\rho(\tau_0)\beta(\tau_0)}}, \qquad \bar{\mathcal{C}}_n(\tau_0) = \frac{e_n^{(2)}(\tau_0)}{4\pi\sqrt{\rho(\tau_0)\beta(\tau_0)}} \ ; \tag{A-8}$$

see Pšenčík (1998a). The initial conditions given by equation (A-8) correspond to a unit force oriented along the coordinate axis x_n. Finally, the B_{mn} in equation (A-7) are determined from the weak anisotropy matrix:

$$B_{mn} = \Delta a_{ijkl}\, e_i^{(m)} e_j^{(3)} e_k^{(3)} e_l^{(n)} \ . \tag{A-9}$$

If the medium is isotropic, $\Delta a_{ijkl} = 0$ and equation (A-3) reduces to the formula for the zeroth-order ray approximation of the S-wave Green's function in isotropic media. If the anisotropy of the medium is strong, the inhomogeneity weak, and the frequency high, the zeroth-order approximation of the QI approach instead yields two independent qS waves that could also be independently described using the ray method for anisotropic media (Kravtsov & Orlov, 1980; Pšenčík, 1998a).

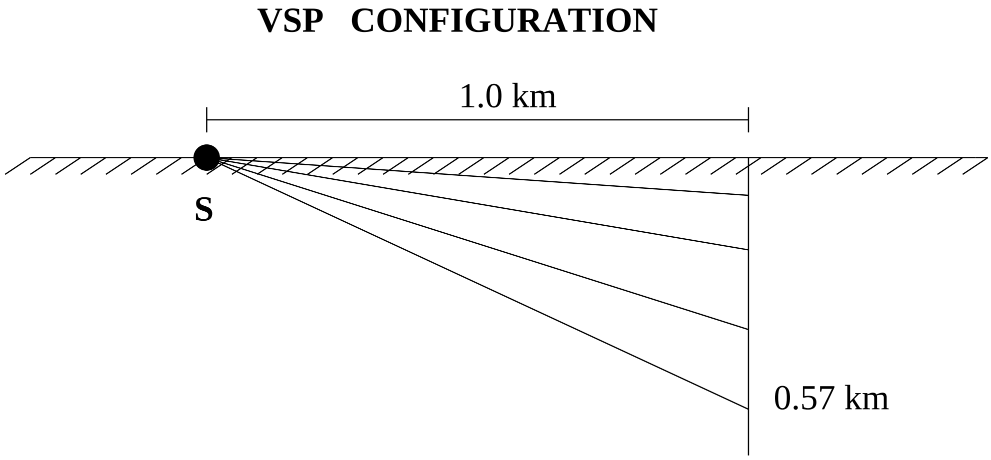

Figure 1: A schematic illustration of the model VSP geometry used for all the examples in this paper.

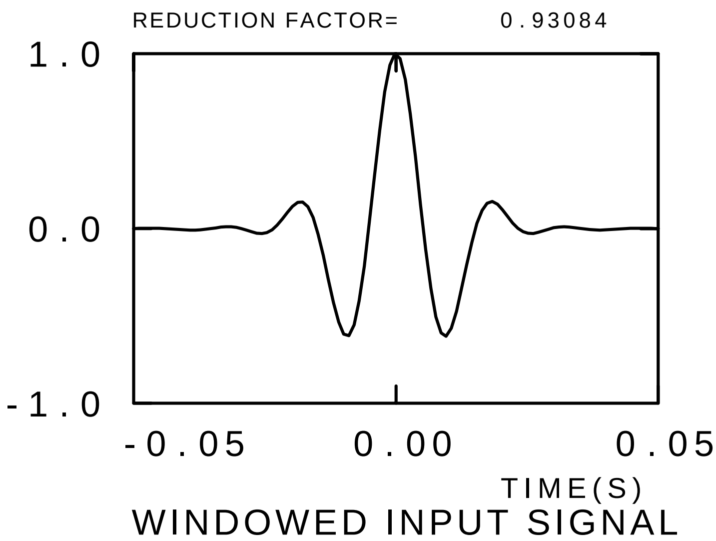

Figure 2: The source wavelet used for the examples in Figures 5, 6, and 8 through 12. The dominant frequency of this wavelet is 50 Hz.

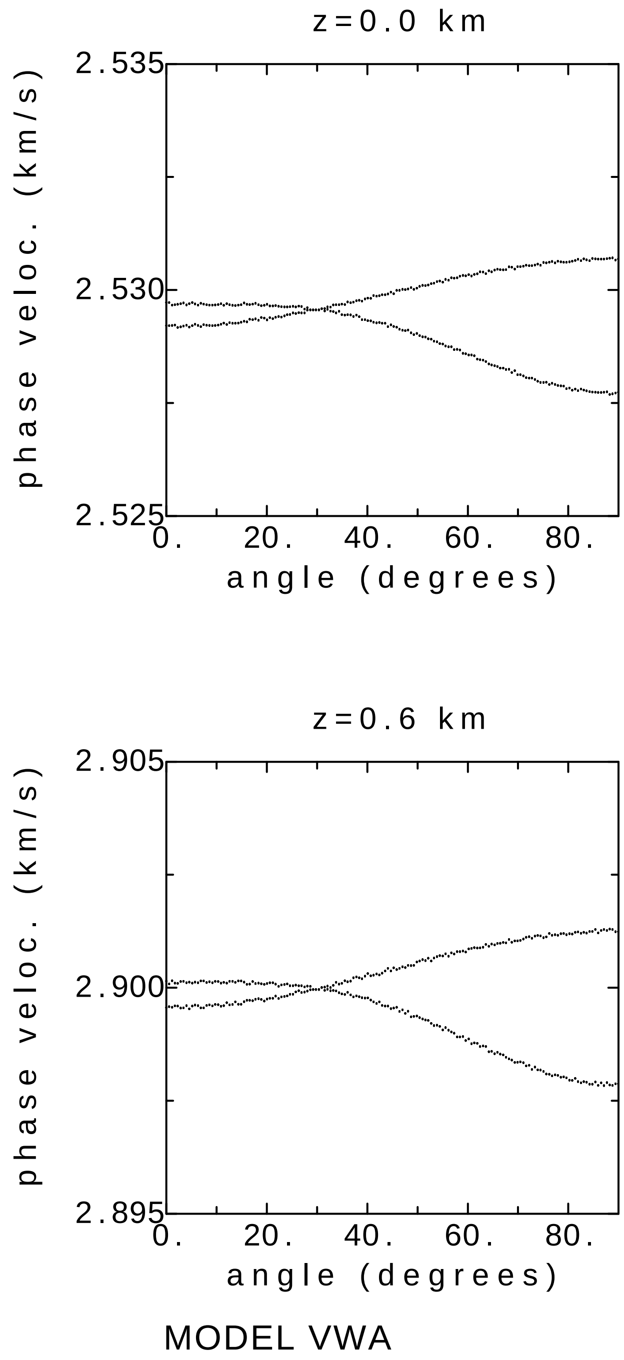

Figure 3: The VWA model: Sections through the qS-wave phase-velocity surfaces in the vertical propagation plane plotted as a function of the angle of incidence (0° = horizontal propagation, 90° = vertical propagation) at depths of 0.0 and 0.6 km. Note the intersection singularity at approximately 30°.

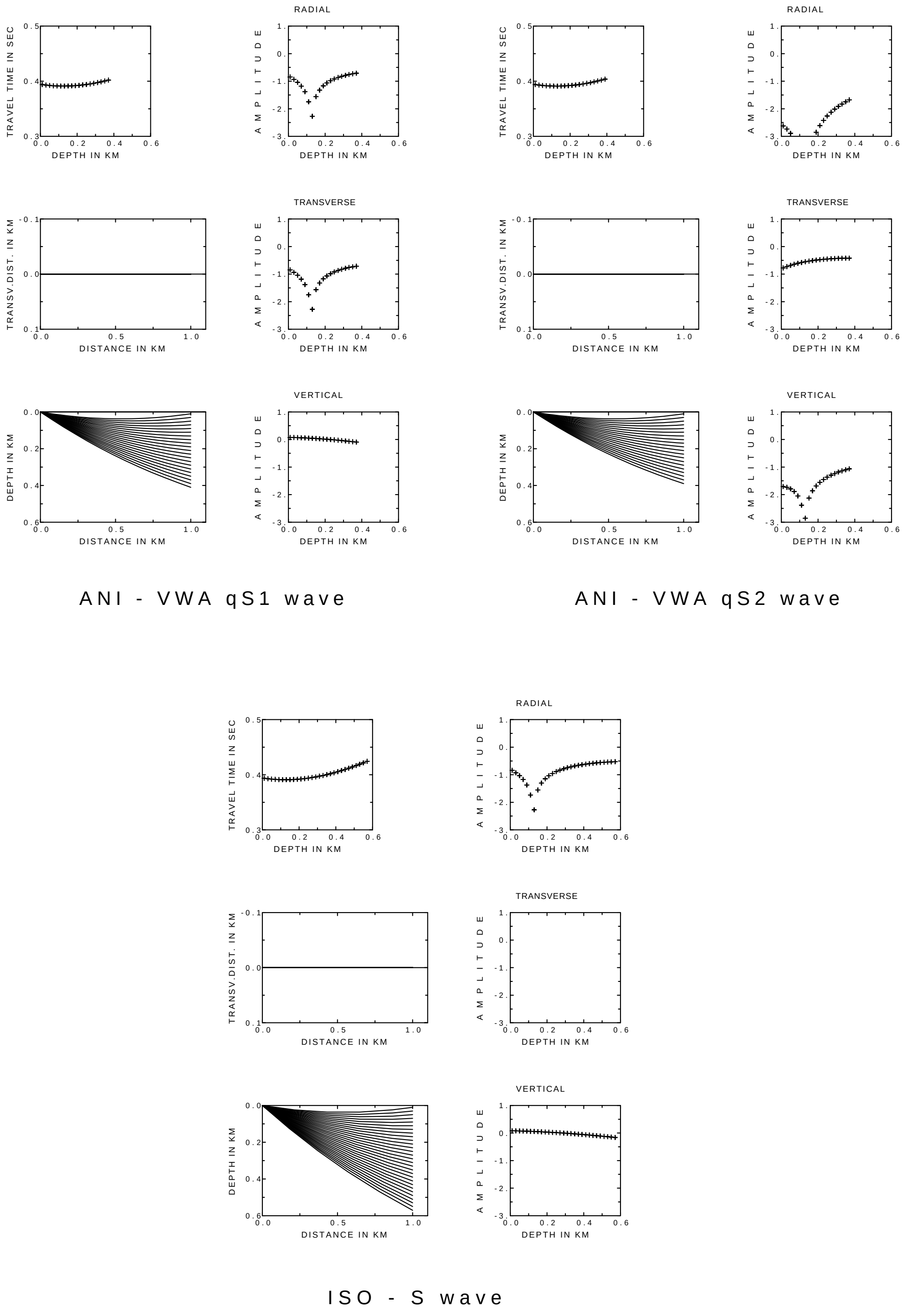

Figure 4: The VWA model (top) and its isotropic approximation (bottom). Ray diagrams and time-distance curves (left columns) and $\log_{10}$ amplitude-distance curves (right columns) for the anisotropic qS waves or the isotropic S wave generated by a vertical point-force source are shown. The results were calculated using both the anisotropic ANI method (top two sets of plots) and the isotropic ISO method (bottom set).

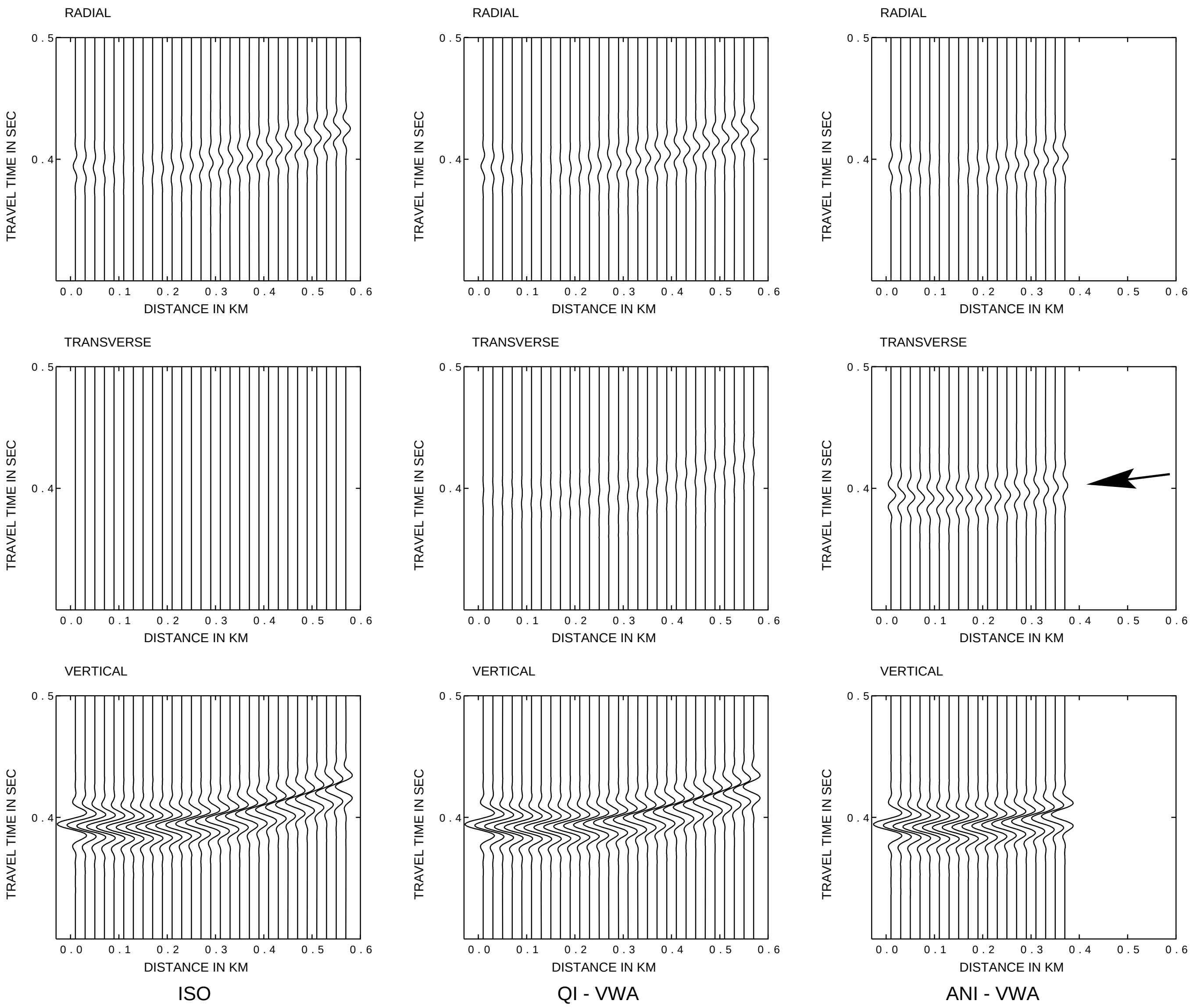

Figure 5: The VWA model: Synthetic seismograms calculated by the ray method for isotropic media (ISO, left), by the QI approach (center), and by the ray method for anisotropic media (ANI, right). The dominant frequency of the source for this example is 50 Hz. The ANI method incorrectly predicts significant amplitudes on the transverse component (see arrow).

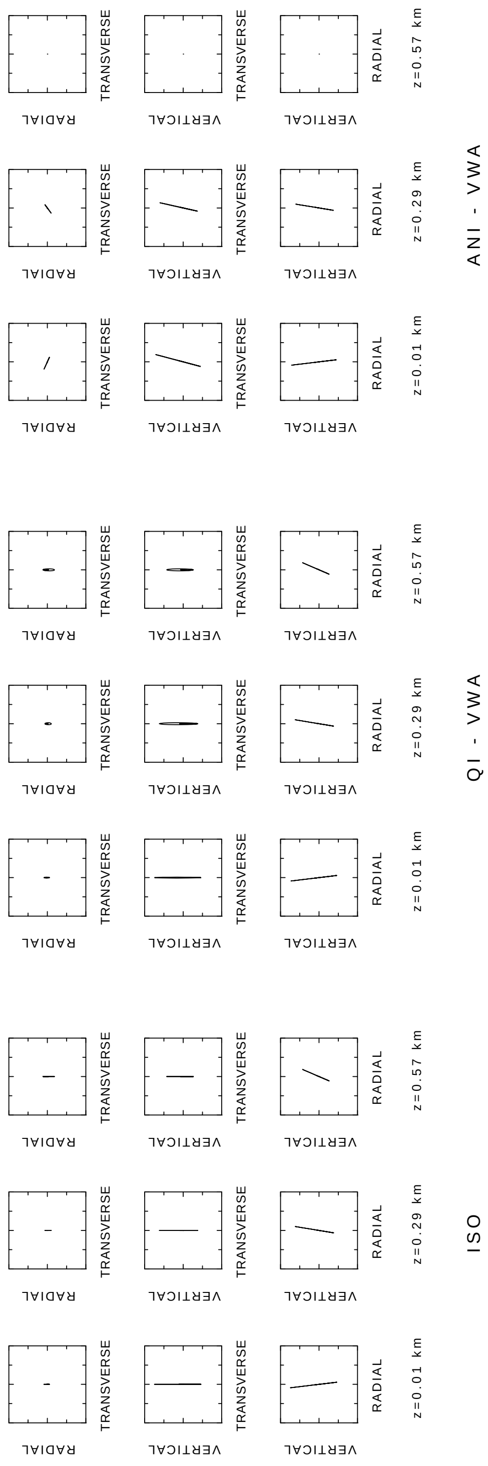

Figure 6: The VWA model: Particle-motion hodograms for receivers at depths $z = 0.01$, 0.29, and 0.57 km calculated using the ray method for isotropic media (ISO, left), the QI approach (center), and the ray method for anisotropic media (ANI, right). The dominant frequency of the source is 50 Hz. The QI and ISO results are very similar for all receivers.

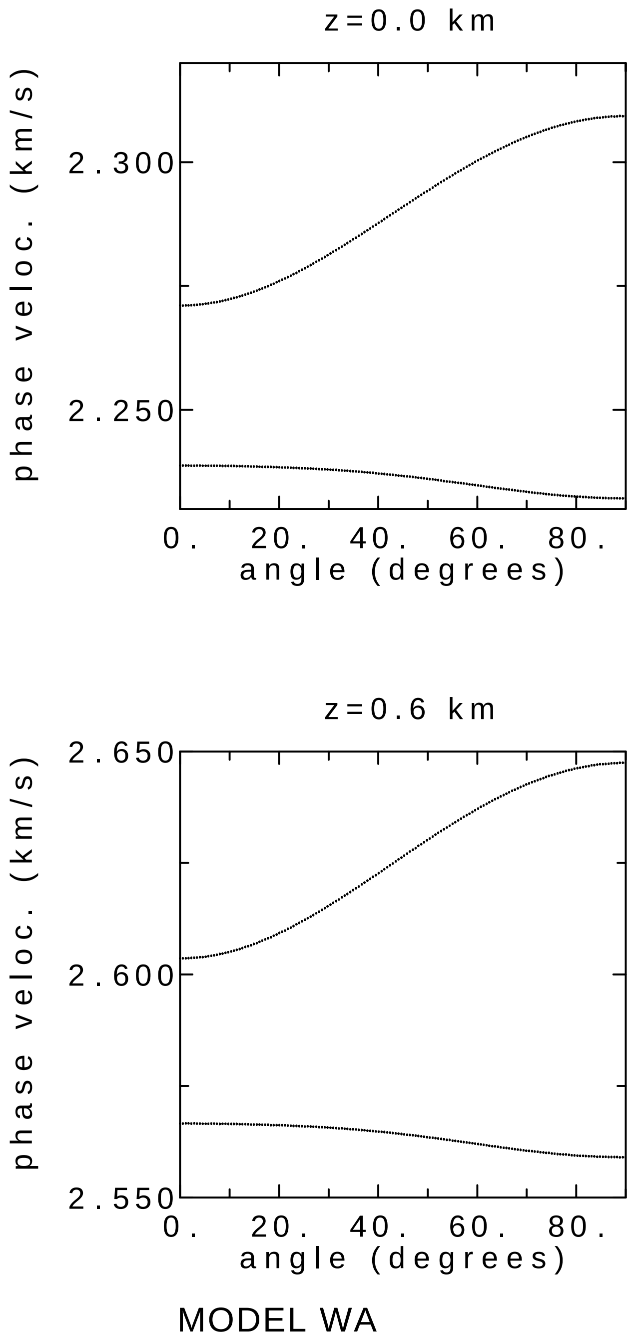

Figure 7: The WA model: Sections through the qS-wave phase-velocity surfaces in the vertical propagation plane plotted as a function of the angle of incidence (0° = horizontal propagation, 90° = vertical propagation) at depths of 0.0 and 0.6 km. The difference in phase velocities between the two qS waves more than doubles as the propagation angle increases from 0° to 90°.

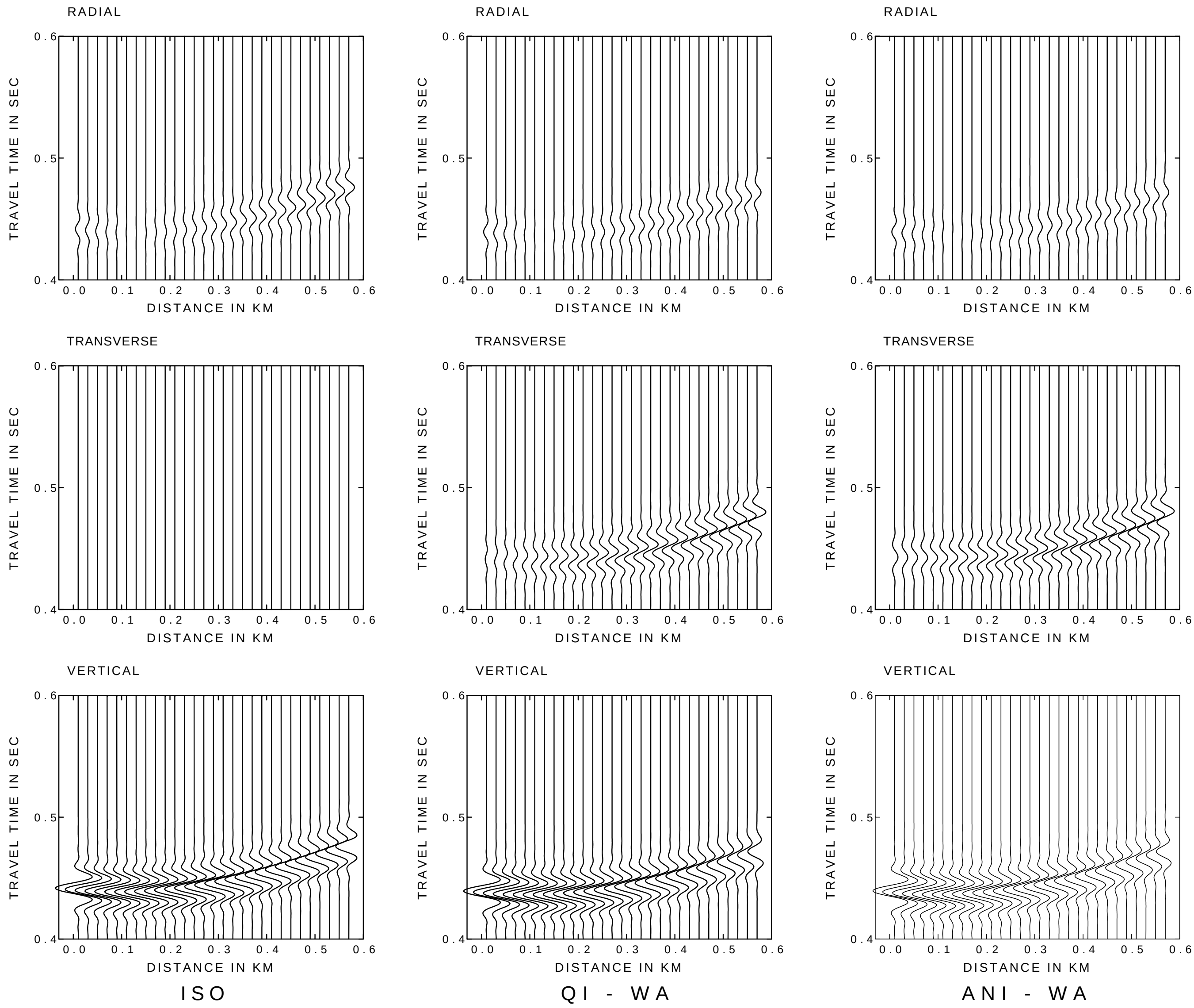

Figure 8: The WA model: Synthetic seismograms calculated by the ray method for isotropic media (ISO, left), by the QI approach (center), and by the ray method for anisotropic media (ANI, right). The dominant frequency of the source is 50 Hz. The QI approach approximates the ISO result for the shallow receiver but the ANI result for the two deeper receivers.

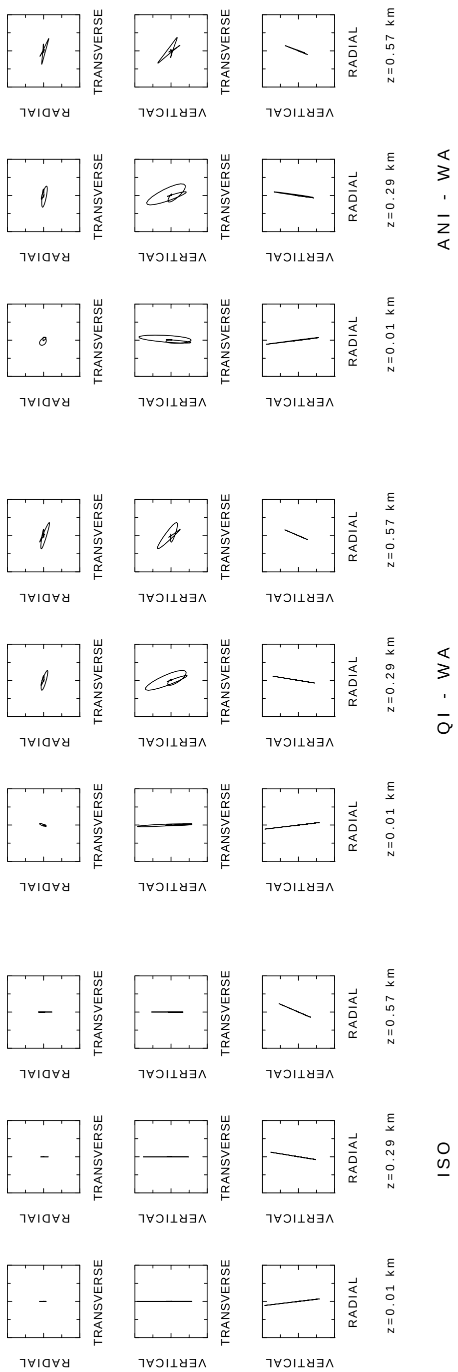

Figure 9: The WA model: Particle-motion hodograms for receivers at depths $z = 0.01$, 0.29, and 0.57 km calculated using the ray method for isotropic media (ISO, left), the QI approach (center), and the ray method for anisotropic media (ANI, right). The dominant frequency of the source is 50 Hz. The QI approach approximates the ISO result for the shallow receiver but the ANI result for the two deeper receivers.

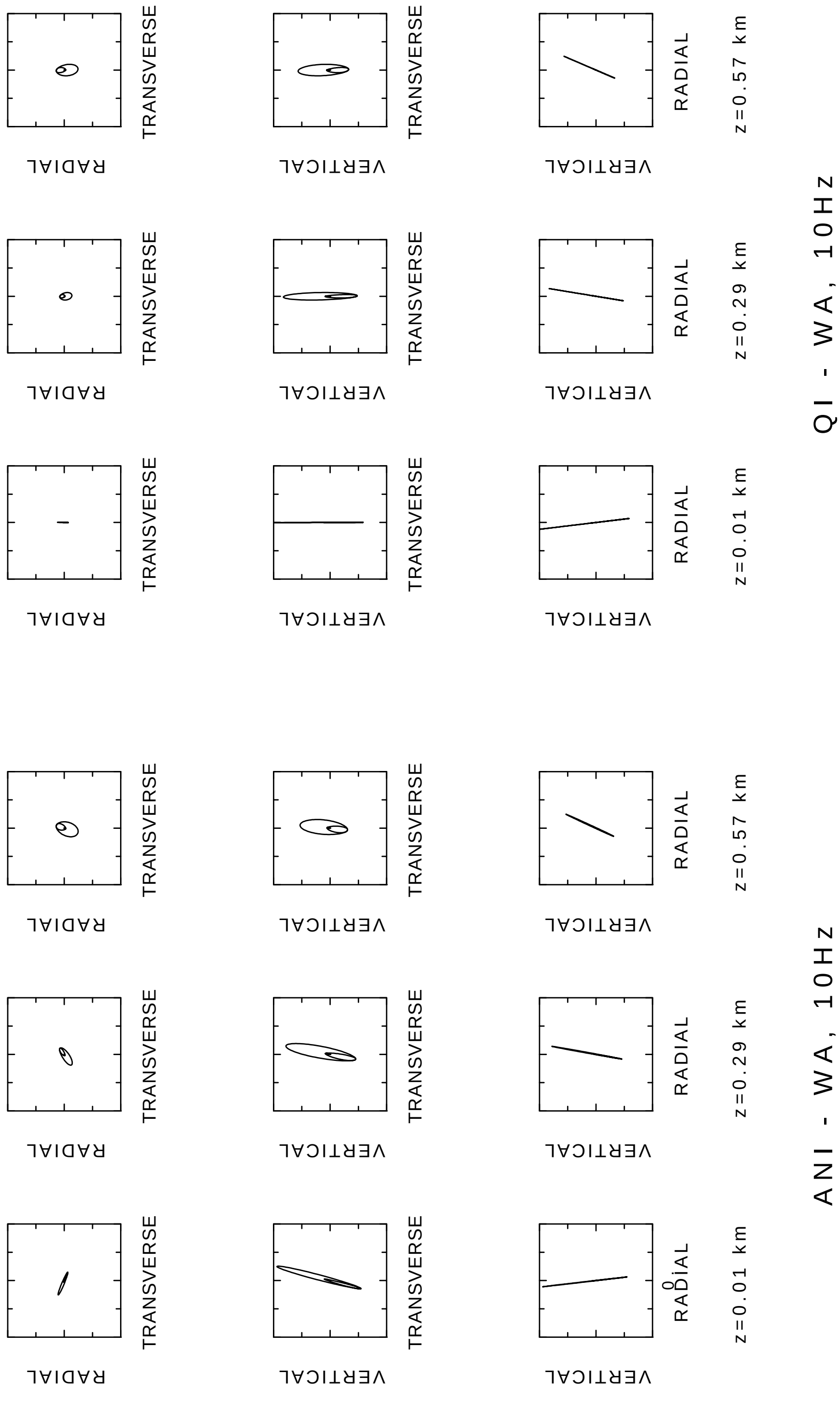

Figure 10: The WA model: Particle-motion hodograms for the same receivers as in Figure 9, calculated using the ray method for anisotropic media (ANI, left) and the QI approach (right). The dominant frequency of the source has been lowered to 10 Hz. At this lower frequency, the QI results appear more similar to the ISO results shown in Figure 9.

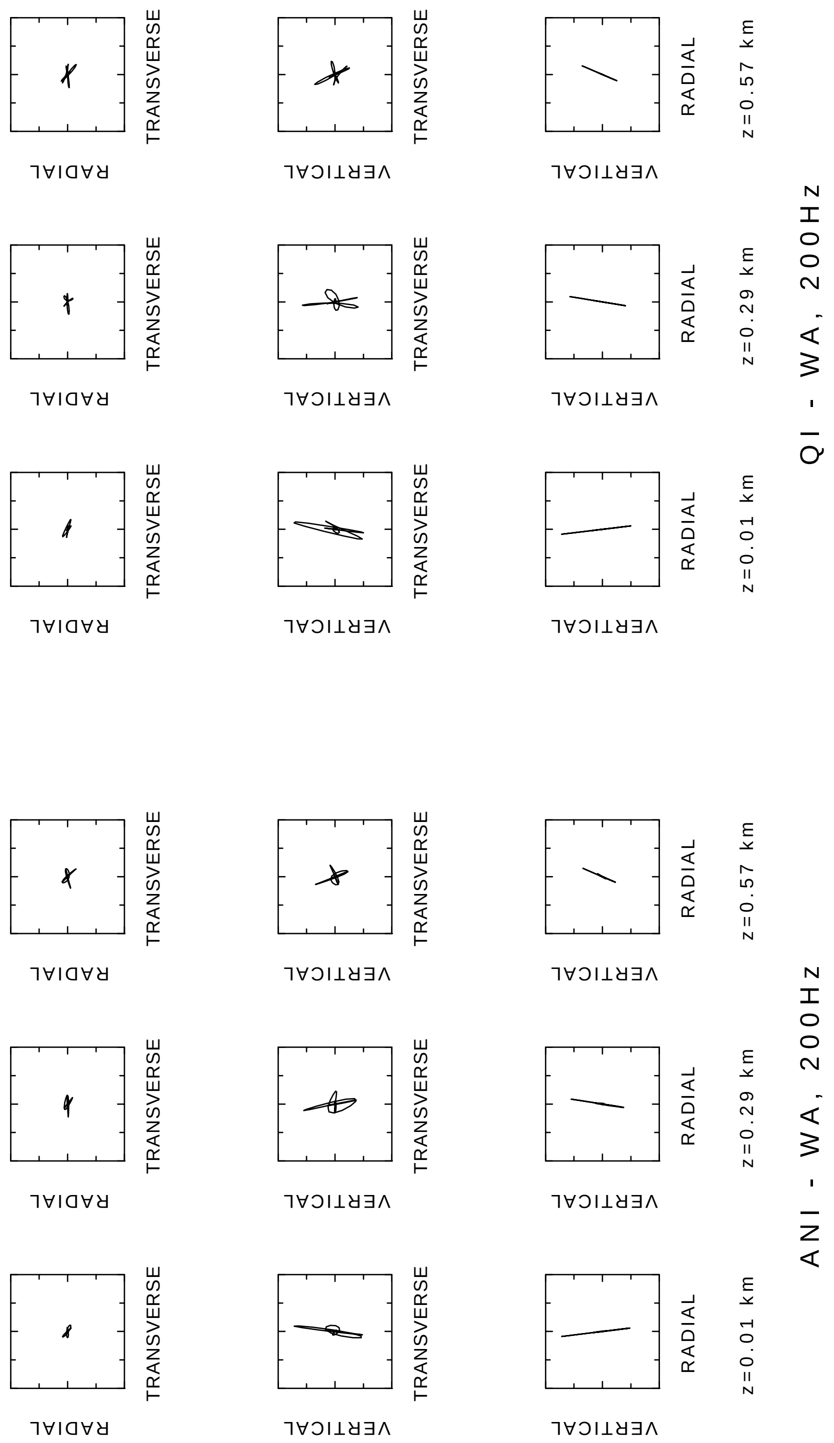

Figure 11: The WA model: Exactly as Figures 9 and 10, but the dominant frequency of the source has been increased to 200 Hz. The QI result is now more similar to the corresponding ANI result for all depths. The qS waves are clearly separated at the deeper receivers.

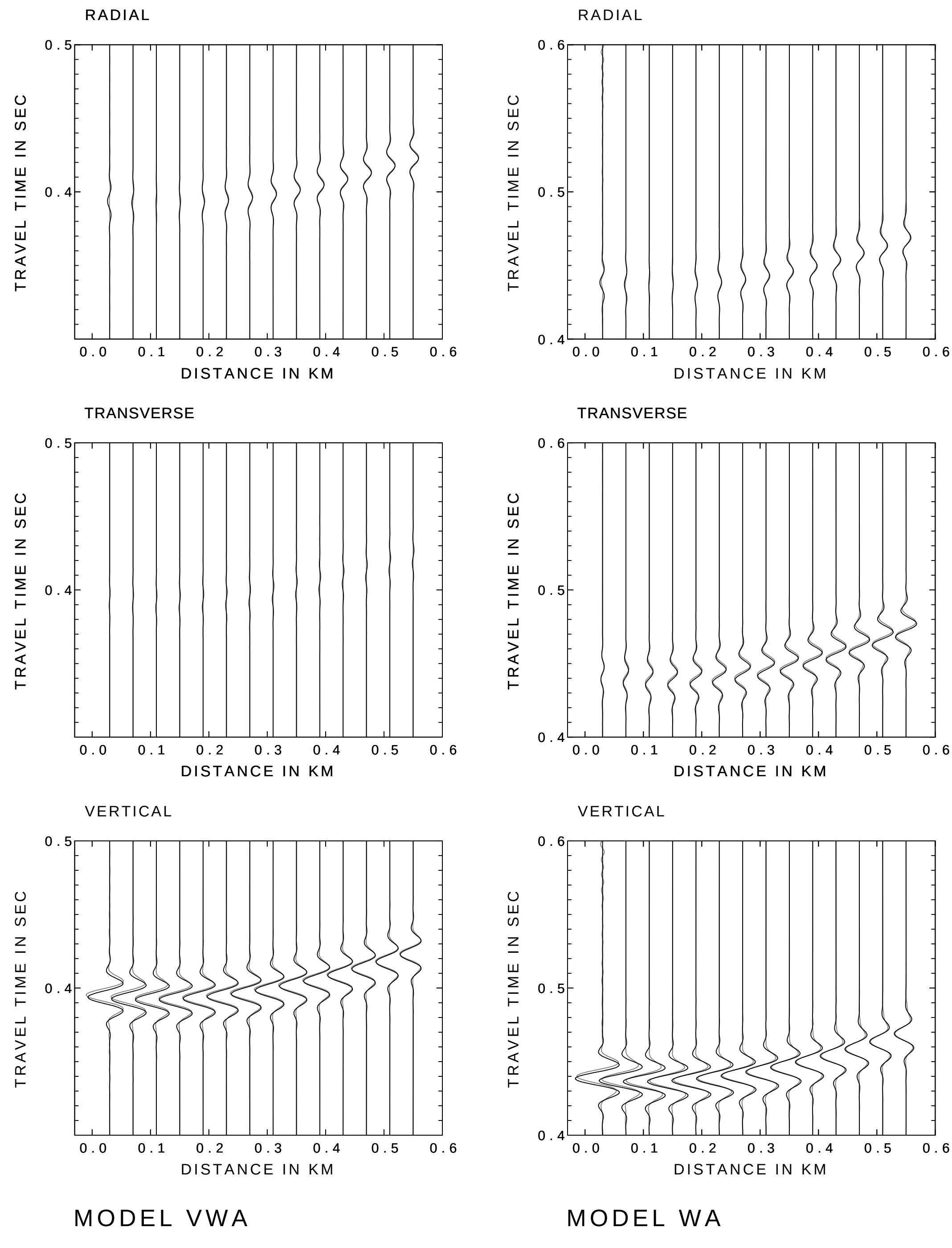

Figure 12: Comparison of the synthetic seismograms calculated using the the QI approach (dark lines) and the reflectivity method (grey lines) for the VWA model (left column) and the WA model (right column). Only seismograms for even-numbered receivers are shown, so the individual waveforms can be better seen.